Volume 1 | Number 1 | Jan 2013 | Pages 1–100

Nanoscale

www.rsc.org/nanoscale

ROYAL SOCIETY OF CHEMISTRY

This is an *Accepted Manuscript*, which has been through the Royal Society of Chemistry peer review process and has been accepted for publication.

Accepted Manuscripts are published online shortly after acceptance, before technical editing, formatting and proof reading. Using this free service, authors can make their results available to the community, in citable form, before we publish the edited article. We will replace this *Accepted Manuscript* with the edited and formatted *Advance Article* as soon as it is available.

You can find more information about *Accepted Manuscripts* in the **Information for Authors**.

Please note that technical editing may introduce minor changes to the text and/or graphics, which may alter content. The journal's standard **Terms & Conditions** and the **Ethical guidelines** still apply. In no event shall the Royal Society of Chemistry be held responsible for any errors or omissions in this *Accepted Manuscript* or any consequences arising from the use of any information it contains.

Journal Name

Dynamic Article Links ▶

ARTICLE TYPE

Multifunctional Fe$_3$O$_4$@TiO$_2$@Au Magnetic Microspheres as Recyclable Substrates for Surface-Enhanced Raman Scattering

Xiaoqing Zhang, Yihua Zhu,* Xiaoling Yang, Ying Zhou, Yifan Yao and Chunzhong Li*

Herein, we demonstrate the design and fabrication of multifunctional triplex Fe$_3$O$_4$@TiO$_2$@Au core-shell magnetic microspheres (MS), which show excellent surface enhanced Raman scattering (SERS) activity with high reproducibility and stability. In addition, due to possessing excellent catalytic properties, the as-prepared Fe$_3$O$_4$@TiO$_2$@Au magnetic MS can clean themselves by photocatalytic degradation of target
10 molecules adsorbed onto the substrate under irradiation with visible light, and can be re-used for several cycles with convenient magnetic separability. The influence of size and distribution of Au nanoparticles (NPs) on the Fe$_3$O$_4$@TiO$_2$ beads are investigated. The optimized samples employing Au NPs with 15 nm size and areal density of about 2120 Au NPs on every MS show the best SERS activity and recyclable performance. The experimental results show that these magnetic MS indicated a new route in eliminating
15 the single-use problem of traditional SERS platform and exhibit its feasibility as an analytical tool for detection of different molecular species.

1. Introduction

As a powerful spectroscopic technique, surface-enhanced Raman scattering (SERS) has been attracting increasing interests due to
20 its wide applications in various fields, including analytical chemistry, medical science, life science and the characterization of trace chemical species.[1-5] It relies on the exploitation of surface plasmon-polarition near-field generated by interaction of a light source with an SERS-active substrate, which is generally made of
25 noble metals (Au, Ag and Cu) with multiple shapes (such as nanoparticles (NPs), nanorods, nanocubes and nanoflowers).[6-10] The enhancement factors of SERS can reach as large as 10^{14}-10^{15}.[2] Furthermore, in the last several years, great progress has been made in the design and synthesis of various noble-metal
30 nanostructured materials as Raman signal enhancing agents. For instance, nanocomposite materials composed of SERS-active NPs and zero-, one- and two-dimensional nanostructured support materials have been shown to exhibit superior SERS activity.[11-15] Among these reports, the dielectric-core/metallic-shell geometry
35 can offer unique advantages for SERS, as it allows concentrating the scattering electromagnetic field at the metal surface.[16-19] In particular, TiO$_2$ has been exploited as a potential candidate for fabrication of SERS substrates since the TiO$_2$-assisted enhanced charge transfer from the metal to the probe molecule.[20,21]
40 However, from the application viewpoint, not only strong enhancement factors but also good stability, homogeneity and reproducibility are necessary for an efficient SERS substrates.

Aside from the enhancement, with the progress of SERS, developing the SERS substrates with stability or reproducibility is
45 required. It has been shown recently that fabrication of periodic arrays of NPs by nanosphere lithography, electron beam lithography or focused ion beam milling are the most common

ways to avoid these defects.[22] For instance, Zhao and co-workers prepared nanoscale Ag semishell array with tunable interparticle
50 distance by combining nanosphere lithography with reactive ion etching.[23] The as-prepared substrates exhibit homogeneity and good enhancing ability. However, most are complicated to be fabricated and require sophisticated and specialized apparatus. In addition, most of the traditional SERS substrates are single use,
55 and considering the preciousness of the noble metals, these SERS substrates can not be fully explored or recognized as a routine analytical technique. Therefore, the research has been focused on developing recyclable SERS-active substrates, which have photocatalytic activity as well as SERS property, since it can not
60 only decrease the waste of resources, but also enhance the efficiency of SERS substrates. Furthermore, environmental pollution has become a severe problem, from the environmental viewpoint, SERS-active substrate has potential need for the treatment of contamination as well as for detection of the organic
65 pollution.[24] Several workgroups have reported recyclable SERS substrate, Ivano and co-workers investigated a simple and cheap way to fabricate Au-coated ZnO nanorods, the as-prepared substrates show excellent SERS and recyclable performance.[17] However, compared to ZnO, TiO$_2$ is considered to be one of the
70 suitable materials for photocatalyst due to its nontoxicity, biological inertness, chemical stability and low-cost character.[25,26] Asefa and co-workers synthesized a porous TiO$_2$-Ag core-shell nanocomposite material, the as-prepared nanocomposite material was shown to serve as an efficient self-cleaning SERS substrate.[27]
75 However, these nanocomposites are sometimes separated by complex methods, which limits their use. To avoid these defects, magnetic Fe$_3$O$_4$ particles have been often introduced to functionalize core-shell particles due to their unique separable

Nanoscale Accepted Manuscript
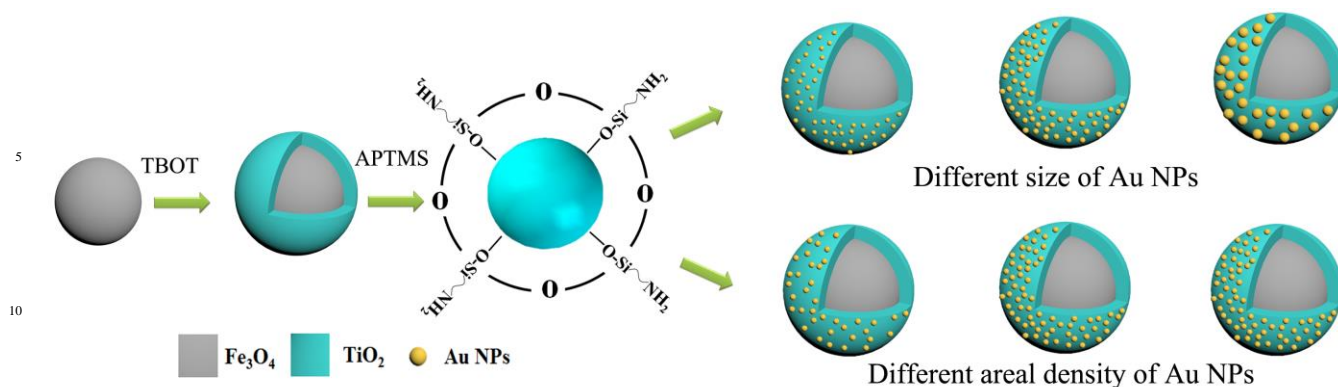
Figure 1. Schematic diagram and structural model of the multifunctional $Fe_3O_4@TiO_2@Au$ MS.

feature that makes it possible to realize convenient recycling of novel metals.[28-31] And considering the stability, Au is much more oxidation-resistant than Ag so that can prolong the substrate lifetime.[31] So on the basis of the above analysis, we intend to make use of the characteristics of Fe_3O_4, TiO_2 and Au nanomaterials in the synthesis of a multifunctional SERS-active substrates, which can be applied to the recyclable SERS-active substrates.

Herein, we report the design and synthesis of stable, homogeneous, reproducible and recyclable Fe_3O_4-TiO_2-Au based SERS substrates in powder form. The as-prepared multifunctional microspheres (MS) have a Fe_3O_4 core, TiO_2 interlayer and Au shell with different size range and areal density of the Au shell. These SERS-active substrates with unique multicomponent nanostructure, designated $Fe_3O_4@TiO_2@Au$ (as shown in figure 1), are fabricated by conformal coating Fe_3O_4 MS with TiO_2 by sol-gel process, and then the $Fe_3O_4@TiO_2$ MS are modified by 3-Aminopropyltrimethoxysilane (APTMS), followed by coating with a layer of citrate-stabilized Au NPs. The areal density of Au NPs can be effectively controlled by changing the coating time of Au. The SERS activities of these MS have been tested by using Rhodamin 6G (R6G) as a probe molecule. The unique nanostructure makes the MS novel stable, homogeneous, recyclable and high-enhancement effect for Raman detection.

2. Experimental

2.1. Materials

3-Aminopropyltrimethoxysilane (APTMS) were purchased from Sigma-Aldrich Chemicals Co. $FeCl_3.6H_2O$, Chloroauric acid, trisodium citrate, citric acid, sodium acetate, tetrabutyl titanate (TBOT), ethanol, ethylene glycol, NH_4F, aqueous ammonia (28 wt%), Rhodamine 6G (R6G) were of analytical grade and purchased from Shanghai Chemical Corp. All chemicals were used as received. Ultrapure water (18 MΩ cm^{-1}) was used for all experiments.

2.2. Synthesis of Fe_3O_4 NPs

Fe_3O_4 MS with an average size of ~300 nm were synthesized using the method introduced by Liu *et al*.[33] In a typical synthesis, 3.25 g of $FeCl_3.6H_2O$, 1.3 g of trisodium citrate and 6.0 g of sodium acetate were dissolved in 100 mL of ethylene glycol with magnetic stirring. This mixture was then transferred and sealed

into a Teflon-lined stainless-steel autoclave (200 mL in capacity). Then the reaction was allowed to proceed at 200 °C for 10 h. The obtained black products were washed with deionized water and ethanol for 3 times, respectively. Finally, the obtained Fe_3O_4 MS were dried in vacuum for 12 h.

2.3. Synthesis of $Fe_3O_4@TiO_2$ NPs

The $Fe_3O_4@TiO_2$ core-shell MS with uniform porous TiO_2 shell were performed following a protocol described by Zhao *et al*.[34] In a typical synthesis, 0.075 g of Fe_3O_4, 0.3 mL of aqueous ammonia (28 wt%) were dissolved in 90 mL of ethanol and stirred for 15 min at 600 rpm at 45 °C. Then 0.75 mL of TBOT previously dissolved in 10 mL of ethanol, which was introduced drop by drop with continuous stirring, and the reaction was continued for 24 h under continuous mechanical stirring. The resultant products were separated and collected, followed by washing with ethanol and water for 3 times, respectively. The obtained powders were dried in vacuum for 12 h. To improve crystallinity, 0.4 g of $Fe_3O_4@TiO_2$ MS and 0.37 g of NH_4F were mixed with 66 mL of ethanol and 34 mL of H_2O under mechanical stirring for 60 min. The mixture was hydrothermally treated at 180 °C in a Teflon-lined stainless steel autoclave (200 mL in capacity) for 24 h. The as-prepared product was washed with ultrapure water for 3 times to remove any ionic impurities, and dried at 80 °C overnight. Finally, the obtained $Fe_3O_4@TiO_2$ MS were dispersed in 200 mL of ethanol and 0.5 mL of APTMS, and the mixture was refluxed at 85 °C for 4 h. The resultant APTMS-modified $Fe_3O_4@TiO_2$ beads were washed with ethanol for 3 times and redispersed in 100 mL of ethanol.

2.4. Synthesis of $Fe_3O_4@TiO_2@Au$ NPs

Citrate-stabilized Au NPs of different sizes (5, 15 and 30 nm) were prepared according to the reported methods.[35,36] The PH of the Au NPs and $Fe_3O_4@TiO_2$ solution were adjusted to 5.0 by titration with 0.01 M HCl. Then 2.0 mL of $Fe_3O_4@TiO_2$ solution was added dropwise to 200 mL of the raw gold NPs solution and stirred for different time (5, 10, 15 min) to control the areal density of Au NPs on the surface of the $Fe_3O_4@TiO_2$ MS.

2.5. Characterization

To demonstrate the overall uniformity and morphology of the particles, the samples were examined by transmission electron microscopy (TEM) using a JEOL 2011 microscope (Japan) and scanning electron microscope (SEM) images using a JEOL JSM-

6360LV microscope (Japan). The crystalline structure was investigated by X-ray power diffraction (RIGAK, D/MAX 2550 VB/PC, Japan).

2.6. Measurement of SERS activity of $Fe_3O_4@TiO_2@Au$ NPs

Raman spectra were recorded on an inVia Raman microprobe (Renishaw Instruments, England) with 785 nm laser excitation at room temperature, equipped with Peltier charge-coupled device detectors and a Leica microscope. An accumulation times of 10 s was used for both Spectra. Power at the sample was typically 150 mW. A long working distance 50× objective was used to collect the Raman scatter signal. All of the Raman spectra presented in this work consisted of an average of three spectra, which collected at three different positions over the samples. To analyze the performance of the as-prepared $Fe_3O_4@TiO_2@Au$ MS, R6G was used as a model analyte. The different concentrations of Rd 6G aqueous solution were configured into 10^{-2}, 10^{-5}, 10^{-6}, 10^{-7}, 10^{-8}, 10^{-9}, 10^{-10} and 10^{-11} M. In a typical experiment, we put the $Fe_3O_4@TiO_2@Au$ MS in a vial, and the solution of R6G (10 mL) was mixed with the MS in the vial. After 10 min, a magnet was placed under the vial to collect the MS, and then, in situ SERS activity of the solution at the position of onto the magnet was detected.

2.7. Regeneration and photocatalytic activity tests

Photocatalytic reactions for degradation of R6G were carried out in a 250 mL quartz beaker, containing 150 mL of reaction slurry. Agitation was provided by mechanical stirring. The aqueous slurry, prepared with 50 mg different kinds of catalysts (the specific surface area (BET) of P25 is about 50 ± 15 m^2/g, and the BET value of all the as-prepared MS are 50~60 m^2/g) and 2.0×10^{-5} M R6G were stirred in the dark for 30 min to ensure that the dye was adsorbed to saturation on the catalysts. A UV lamp (365 nm, 70 W cm^{-2}) or a high pressure Xenon lamp with a cutoff filter to block the UV light (<400 nm, 50 mW cm^{-2}) was used as the light source, which was placed 10 cm away from the reaction vessel. The photocatalytic reaction was started by turning on the lamp. 3 mL of the mixed suspension was extracted at various irradiation times and the photocatalyst was collected with a magnet. The concentration of residual R6G in the upper clear layer was determined by recording the maximum absorbance of R6G with a UV-vis spectrophotometer.

For regeneration tests, the samples were collected after SERS tests in a 100 mL quartz beaker containing 50 mL of water. Agitation was provided by mechanical stirring. A UV lamp (365 nm, 70 W cm^{-2}) or a high pressure Xenon lamp with a cutoff filter to block the UV light (<400 nm, 50 mW cm^{-2}) was used as the light source, which was placed 10 cm away from the reaction vessel. After irradiation, the samples were collected with a magnet and dried in air for further SERS tests.

3. Results and discussions

3.1. Characterization of the triplex $Fe_3O_4@TiO_2@Au$ core-shell MS

This triplex core-shell $Fe_3O_4@TiO_2@Au$ MS have a Fe_3O_4 magnetic core, a TiO_2 interlayer, and a layer of Au NPs shell. Figure 1 schematically highlights the major steps for the fabrication of $Fe_3O_4@TiO_2@Au$ nanostructures. Fe_3O_4 MS with a diameter of approximately 300 nm were first synthesized through a robust solvothermal reaction (Figure 2a), the magnetic core ensures the easy separating of the SERS substrates from the reaction mixture. A uniform interlayer of TiO_2 with thickness of about 35 nm was coated onto Fe_3O_4 beads (Figure 2b), which ensures the degradation of organic dyes so that the MS can be re-used. Later, the resulting $Fe_3O_4@TiO_2$ core-shell MS were modified with APTMS to render the particle surfaces with amino groups. Finally, mixing the modified core-shell $Fe_3O_4@TiO_2$ MS with citrate-stabilized Au NPs (with different size) leads to the grafting of Au NPs on the surfaces of $Fe_3O_4@TiO_2$ MS (Figure 3). By changing the mixing time, different areal densities of Au NPs on the surface of $Fe_3O_4@TiO_2$ MS were prepared (Figure 6).[37]
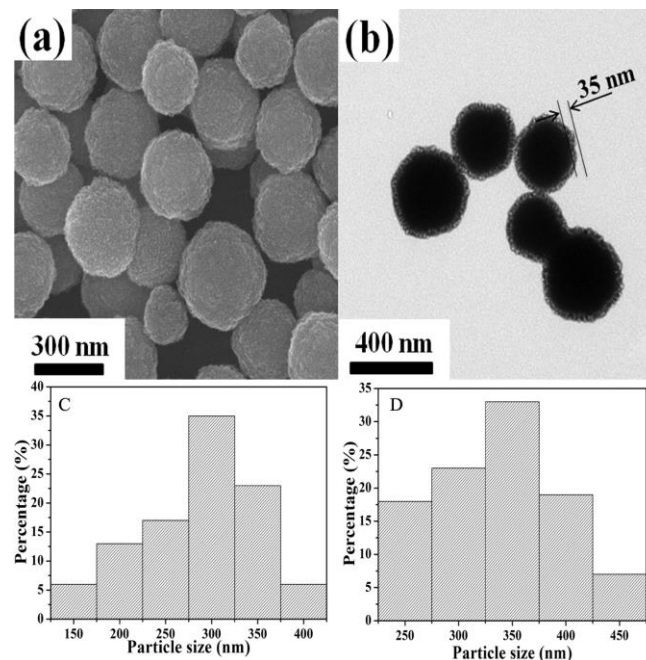
Figure 2. (a) SEM image of Fe_3O_4 MS. (b) TEM image of $Fe_3O_4@TiO_2$ core-shell MS with a uniform TiO_2 shell thickness of 35 nm. (c) Size distribution of the as-prepared Fe_3O_4 MS and (d) $Fe_3O_4@TiO_2$ MS.

Figure 2a and c show the SEM image and particle distribution of Fe_3O_4 MS, revealing that Fe_3O_4 MS have an average particle size of 300 nm. Then, via a sol-gel process of hydrolysis and condensation of TBOT in ethanol/ammonia mixtures, uniform and well-dispersed core-shell $Fe_3O_4@TiO_2$ MS can be obtained, with an average of 35 nm shell thickness. The surface of obtained $Fe_3O_4@TiO_2$ MS was further modified by APTMS to form sufficient amounts of amine functional groups, the strong chemical bonding between Au atoms and N atoms in the amino groups ensures the grafting of Au NPs on the surface of $Fe_3O_4@TiO_2$ MS.[38] As shown in figure 3a, c and e, three samples decorated with Au NPs of size 5, 15, and 30 nm, that is , $Fe_3O_4@TiO_2@Au$ (5 nm), $Fe_3O_4@TiO_2@Au$ (15 nm), and $Fe_3O_4@TiO_2@Au$ (30 nm), were prepared. Figure 3 b, d, and f are the enlarged image of a single MS, which clearly show the 5, 15, and 30 nm Au NPs are successfully decorated on the surface of $Fe_3O_4@TiO_2$ MS. Figure 3 g, h and f are the size distribution of 5, 15, and 30 nm Au NPs decorated on the $Fe_3O_4@TiO_2$ MS. Figure 3 clearly shows that the distribution of Au NPs of $Fe_3O_4@TiO_2@Au$ (5 nm) and $Fe_3O_4@TiO_2@Au$ (15 nm) are

more uniform, however, the aggregation of Au NPs can be found in the sample of $Fe_3O_4@TiO_2@Au$ (30 nm).
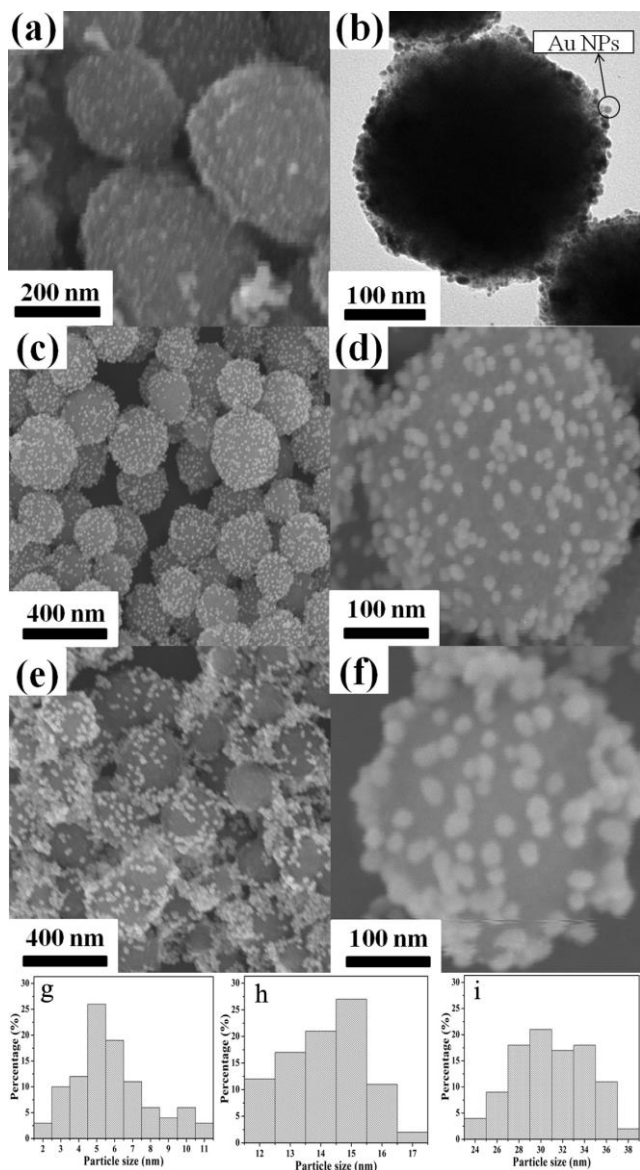
Figure 3. (a) SEM image of $Fe_3O_4@TiO_2@Au$ (5 nm), (c) $Fe_3O_4@TiO_2@Au$ (15 nm), and (e) $Fe_3O_4@TiO_2@Au$ (30 nm). (b) The corresponding magnified TEM images and (d, f) SEM images. (g) Size distribution of 5, (h) 15, and (i) 30 nm Au NPs decorated on the $Fe_3O_4@TiO_2$ MS.

Figure 4 shows X-ray diffraction (XRD) patterns of (a) Fe_3O_4 MS, (b) $Fe_3O_4@TiO_2$ MS and (c) $Fe_3O_4@TiO_2@Au$ (15 nm) MS. Wide-angle XRD patterns show the characteristic broad diffraction peaks indexed to the spinel Fe_3O_4, anatase TiO_2 and cubic phase Au NPs in the composite MS. The specific XRD of Fe_3O_4 is characterized by six peaks positioned at 2θ values of 30.0^o, 35.3^o, 42.9^o, 53.5^o, 57.0^o and 62.4^o, which corresponding to the [220], [311], [400], [422], [511], and [440] lattice planes of the cubic phase of Fe_3O_4 (JCPDS card No. 01-075-0449), respectively. As shown in figure 4 (b), after coated with a ~35 nm TiO_2 and hydrothermal treatment, compared with the patterns of Fe_3O_4, the patterns of the $Fe_3O_4@TiO_2$ show several additional peaks, which can be attribute to the anatase phase of TiO_2. The

extra peaks located at 25.3^o, 37.9^o, 48.0^o and 53.9^o respond to the reflections from the [101], [004], [200], and [105] planes of the anatase phase (JCPDS card No. 01-075-2545). It can be clearly shown in figure 4 (c) that after loading 15 nm Au NPs on the surface of the $Fe_3O_4@TiO_2$ MS, several additional diffraction peaks can be found, which indexed to the cubic phase of Au (JCPDS card No. 00-004-0784). The characteristic XRD patterns of $Fe_3O_4@TiO_2@Au$ (15 nm) MS imply that the current system is suitable for the purpose.
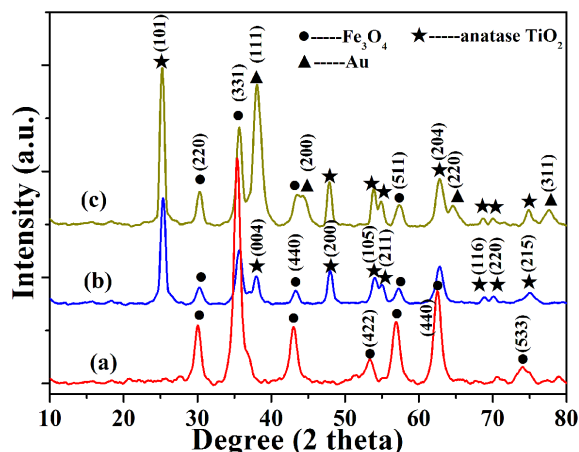

Figure 4. Typical XRD patterns of (a) Fe_3O_4, (b) $Fe_3O_4@TiO_2$ and (c) $Fe_3O_4@TiO_2@Au$ (15 nm) MS.

Figure 5 shows the magnetic hysteresis loops of the bare Fe_3O_4, $Fe_3O_4@TiO_2$, and $Fe_3O_4@TiO_2@Au$ (15 nm) MS at room temperature. As can be seen, they exhibited superparamagnetic behavior and little hysteresis, remanence and coereivity due to the fact that the particles were composed of ultrafine magnetite nanocrystals. The magnetization of Fe_3O_4 MS is about 40.1 emu/g, and that of $Fe_3O_4@TiO_2$ and $Fe_3O_4@TiO_2@Au$ (15 nm) are 34.5 and 26.5 emu/g, respectively. The little decrease in magnetization is mainly due to the decrease in the density of Fe_3O_4 in the obtained composites after coated with TiO_2 and Au. However, the $Fe_3O_4@TiO_2@Au$ (15 nm) still showed strong magnetization, which suggested their suitability for magnetic separation.
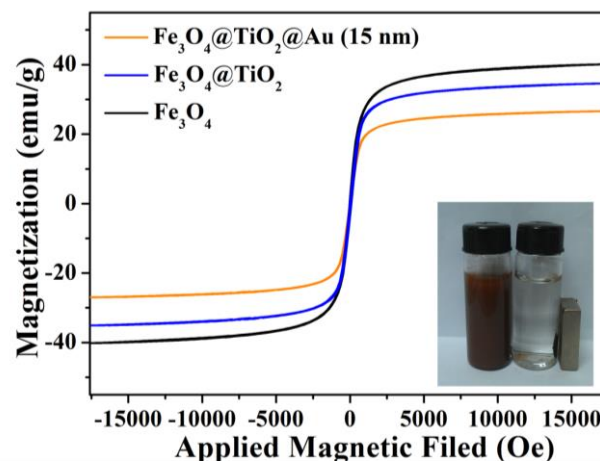
Figure 5. Magnetization curves of the Fe_3O_4, $Fe_3O_4@TiO_2$ and $Fe_3O_4@TiO_2@Au$ (15 nm) MS, respectively. The inset pattern is a photograph of the magnetic separation.
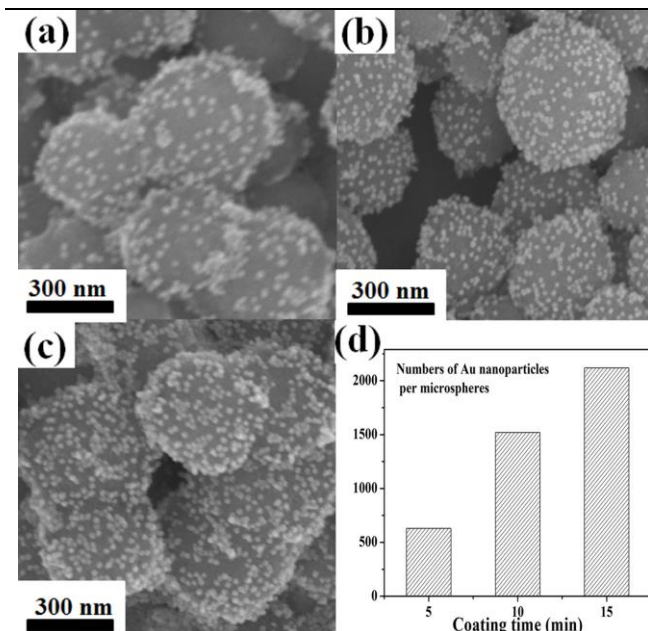
Figure 6. SEM image of Fe₃O₄@TiO₂@Au MS with different Au NPs coating time, (a) 5 min, (b) 10 min and (c) 15 min. (d) Roughly estimated Au NPs on per Fe₃O₄@TiO₂ MS with different Au NPs coating time.

Considering the homogeneity and reproducibility of the SERS substrates, the effect of the areal density of Au NPs on Fe₃O₄@TiO₂ surface was studied using a series of Fe₃O₄@TiO₂@Au (15 nm) , where the density was controlled by changing the coating time of the Fe₃O₄@TiO₂ beads in Au solution. As shown in figure 6 a-c, with the increasing of the coating time, the density of Au NPs gradually becomes larger. By assuming that a uniform distribution of Fe₃O₄@TiO₂ MS with an average particle size of 370 nm as obtained from Figure 2, and uniform distribution of Au NPs as obtained from Figure 6, the number of Au NPs on every Fe₃O₄@TiO₂ MS can be roughly

estimated (Figure 6 d), and the samples were denoted by Fe₃O₄@TiO₂@Au (630/MS), Fe₃O₄@TiO₂@Au (1520/MS), and Fe₃O₄@TiO₂@Au (2120/MS), respectively. However, too long coating time will lead to the aggregation of Au NPs.

3.2. SERS property of the triplex Fe₃O₄@TiO₂@Au core-shell MS

The multifunctional properties of the as-prepared Fe₃O₄@TiO₂@Au MS possess including SERS ability and photocatalytic activity will be demonstrated through a series of experiments. It should me mentioned that because the core-shell MS have the magnetic Fe₃O₄ core, the Fe₃O₄@TiO₂@Au MS could be collected by magnet easily. First, the function of SERS application was tested using R6G as a target molecule due to its well-established vibrational features, and an excitation light source of 785 nm was used. As shown in figure 7 a, the Fe₃O₄@TiO₂@Au MS were added into a vial, a magnet was placed under the vial to collect the MS, and then, in suit SERS activity of the solution at the position of onto the magnet was detected. Generally, the plasmon resonance properties of noble metal NPs are strongly dependent on their size and leavel of aggregation, so the sizes and areal densities of Au NPs on the surface of Fe₃O₄@TiO₂ MS are the two main factors affecting SERS activity. In our study, we choose different sizes of Au NPs and different areal densities to study the SERS activity of the as-prepared multifunctional MS.

The effect of the size of Au NPs was studied by comparing the SERS activities of Fe₃O₄@TiO₂@Au(5 nm), Fe₃O₄@TiO₂@Au (15 nm), and Fe₃O₄@TiO₂@Au(30 nm), and the coating time of Au NPs on the surface of Fe₃O₄@TiO₂ are all 10 min. It should be mentioned that, for 5 nm and 30 nm Au NPs, the coating time more than 10 min will lead to a huge aggregation of Au NPs on the surface of Fe₃O₄@TiO₂. As shown in figure 7 b, the Raman bands at about 1648, 1572, 1509, 1360, 1190, 772 , and 610 cm⁻¹ can be attribute to the xanthene ring stretch, ethylamine group
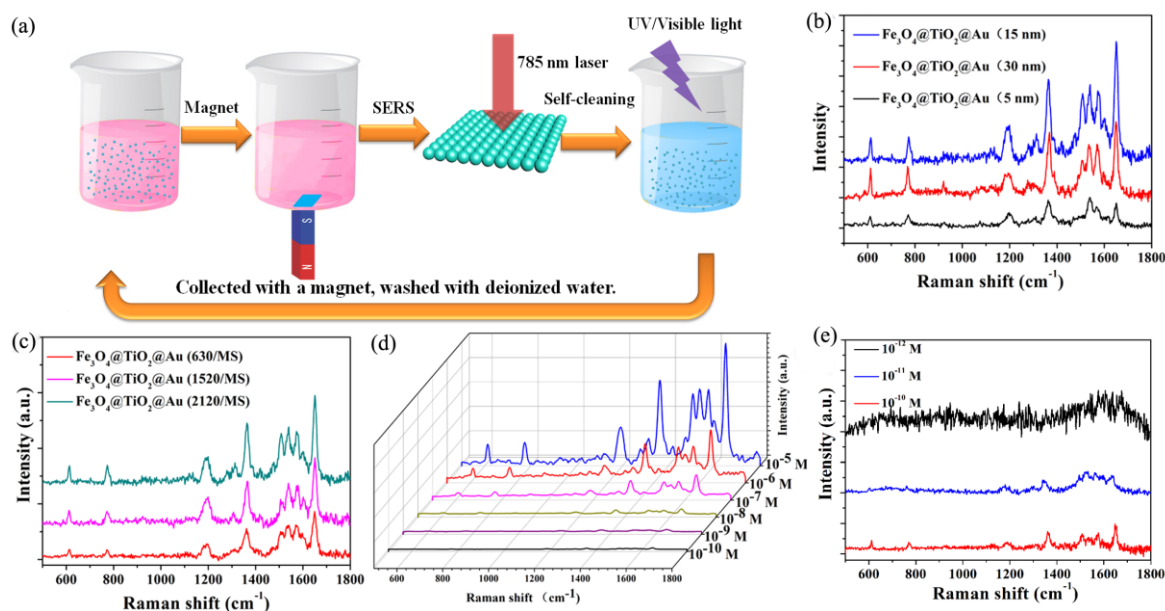
Figure 7. (a) Schematic illustration of in situ SERS detection of R6G adsorbed on Fe₃O₄@TiO₂@Au MS and its recyclable process. SERS spectra of 1×10⁻⁶ M R6G molecules on Fe₃O₄@TiO₂@Au MS (b) with different size of Au NPs and (c) with different areal density of Au NPs (15 nm). (d,e) SERS spectra of R6G molecules on Fe₃O₄@TiO₂@Au (2120/MS) at seven different concentration (1×10⁻⁵ to 1×10⁻¹¹ M).
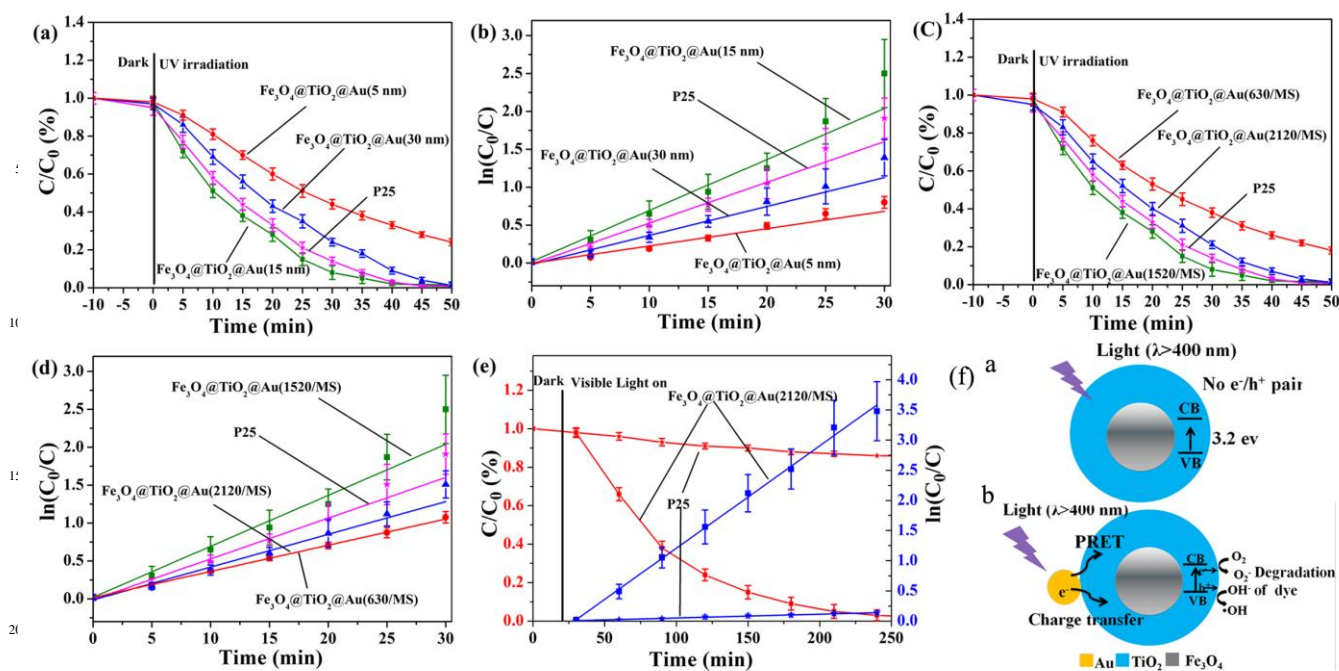
Figure 8. Photocatalytic degradation study of R6G on $Fe_3O_4@TiO_2@Au$ MS (a) with different size of Au NPs and (c) with different areal density of Au NPs (15 nm), $\ln(C_0/C)$ versus time line study on $Fe_3O_4@TiO_2@Au$ (b) with different size of Au NPs and (d) with different areal density of Au NPs (15 nm) under UV irradiation. (e) photocatalytic degradation study of R6G and $\ln(C_0/C)$ versus time line study on $Fe_3O_4@TiO_2@Au$ (2120/MS) under visible light irradiation. (f) Mechanism of the photodegradation process of pure TiO_2 and Au coated TiO_2 during the irradiation of visible light.

wag, and carbon oxygen stretch of R6G.[39] The large SERS enhancement obtained from the triplex $Fe_3O_4@TiO_2@Au$ MS is a process that involves electromagnetic enhancement due to the interaction of the excitation wavelength with plasmon excitations in the nanostructures, as well as chemical enhancement of the R6G molecules adsorbed onto the gold-coated MS. It can be found that $Fe_3O_4@TiO_2@Au(15$ nm) shows the best SERS activity. On the basis of the electromagnetic field theory, Au NPs with the size of 30 nm are expected to be more efficient for surface Raman enhancement than that with the size of 15 nm and 5 nm.[40] There are several reasons why $Fe_3O_4@TiO_2@Au(15$ nm) shows the better SERS activity than $Fe_3O_4@TiO_2@Au(30$ nm). Firstly, it is mainly because that a larger size of Au NPs will restrict the accommodation of more Au NPs on the surface of $Fe_3O_4@TiO_2$, leading to a smaller electromagnetic enhancement, a decreased Au surface area to absorb R6G molecules and a reduced charge transfer from Au to the probe molecules. Secondly, as can be seen in figure 3 e, Au NPs are not homogeneously immobilized. Thus, the decrease of SERS signal intensity might be caused by the inhomogeneous distribution of Au NPs on MS. On the other hand, the reason why $Fe_3O_4@TiO_2@Au$ (15 nm) shows the better SERS activity than $Fe_3O_4@TiO_2@Au$ (5 nm) is mainly because small Au NPs, such as 5 nm Au NPs, have little SERS activity due to its weak electromagnetic field even though it can immobilize more Au NPs on the surface of $Fe_3O_4@TiO_2$ MS.

Though $Fe_3O_4@TiO_2@Au(30$ nm) also shows good SERS activity, considering the homogeneity and reproducibility, $Fe_3O_4@TiO_2@Au(15$ nm) was used as a reference system to study the effect of the areal density of Au NPs in the SERS activity. As shown in figure 7 c, among the three samples, that is, $Fe_3O_4@TiO_2@Au$ (630/MS), $Fe_3O_4@TiO_2@Au$ (1520/MS), and

$Fe_3O_4@TiO_2@Au$ (2120/MS), $Fe_3O_4@TiO_2@Au$ (2120/MS) shows the best SERS activity. As discussed above, a larger areal density of Au NPs can increase the Au surface area, which can absorb more target molecules and ensure more charge transfer from Au to the probe molecules. And it also can enlarge the electromagnetic field intensity. On the other hand, as shown in figure 6, the increased areal density of Au NPs can increase the "hot spots" at the junctions between NPs, however, the surface area ratio between hot spot and other Au surface area is also extremely low, therefore, it might be one of the reasons for the enhancement, but not the most important reason. Figure 7 d and e show the concentration-dependent SERS spectra of R6G with typical aromatic ring vibrations. The detection capabilities of these substrates were evaluated with R6G solutions over a wide range of concentration from 10^{-5} to 10^{-11} M.

A reliable calculation of the enhancement factor (*EF*) through the general formula $EF = (I_{SERS}/N_{Surf})/(I_{RS}/N_{Vol})$ (where I_{SERS} and I_{RS} are the Raman signals under SERS and normal conditions, respectively, N_{Vol} is the average number of molecules in the Raman (non-SERS) scattering volume and N_{Surf} is the average number of adsorbed molecules in the SERS scattering volume) cannot be performed due to the absence of data about the number of R6G molecules which are actually adsorbed onto these MS. However, in our experiment, the enhancement factor was roughly estimated by comparing the intensity of the 1648 cm^{-1} peak in the SERS spectrum with that in the normal Raman spectrum according to the equation $EF = (I_{SERS}/I_R) \times (C_R/C_{SERS})$ by using the reference non-SERS sample (10^{-2} M R6G), where I_{SERS} and I_R are the vibration intensities in the SERS and normal Raman spectra of R6G, respectively, and C_R and C_{SERS} are the concentrations of the R6G molecules in the SERS and reference samples.[17] The *EF* of $Fe_3O_4@TiO_2@Au$ (2120/MS) was roughly
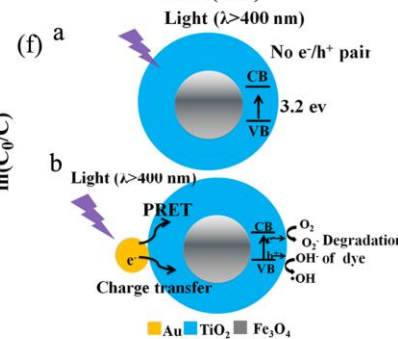
estimated to 8.2×10^8, which is high enough for ultrasensitive detection.

3.3. Photocatalytic activities of the triplex $Fe_3O_4@TiO_2@Au$ core-shell MS

In addition to serving as an effective SERS substrate, $Fe_3O_4@TiO_2@Au$ was considered to possess photocatalytic property. The photocatalytic activity was evaluated by monitoring the dye's characteristic absorption band at 527 nm to measure the degradation rate of R6G under a UV lamp (365 nm, 70 W cm^{-2}) or a high pressure Xenon lamp with a cutoff filter to block the UV light (<400 nm, 50 W cm^{-2}). Figure 8 a and c show the concentration change of the aqueous R6G solution versus UV light irradiation time. As can be seen, the $Fe_3O_4@TiO_2@Au$ MS with systematic variation of size and areal density of Au NPs were studied. And $Fe_3O_4@TiO_2@Au$ (1520/MS) exhibits the best photocatalytic performance. Most of the photocatalytic reactions follow the Langmuir-Hinshelwood adsorption model,[41] and the L-H model can be simplified to a pseudo-first-order expression: $\ln(C_0/C) = kt$ (where C_0 and C are the initial concentration and the concentration of R6G at the exposure time, t, respectively, and k is the linear plots of $\ln(C_0/C)$ versus irradiation time t are attained (as shown in Figure 6b and d), and the photocatalytic reaction rate of $Fe_3O_4@TiO_2@Au$(5 nm), $Fe_3O_4@TiO_2@Au$(15 nm), $Fe_3O_4@TiO_2@Au$(30 nm) and P25 are 0.032, 0.068, 0.041 and 0.056 min^{-1}, respectively. The photocatalytic reaction rate of $Fe_3O_4@TiO_2@Au$ (630/MS), $Fe_3O_4@TiO_2@Au$ (1520/MS), and $Fe_3O_4@TiO_2@Au$ (2120/MS) are 0.037, 0.068 and 0.042 min^{-1}, respectively. Though the sample of $Fe_3O_4@TiO_2@Au$ (1520/MS) shows the best photoatalytic activity, the sample of $Fe_3O_4@TiO_2@Au$ (2120/MS) also shows excellent property to degrade the target molecules.

Furthermore, it has been shown recently that metal NPs, such as Au and Ag, embedded in the matrix of TiO_2 can enhance the photocatalytic activity of TiO_2 under visible light irradiation.[42-44] In order to study the photocatalytic activity of as-prepared MS under visible light, a 150 W high pressure Xenon lamp with a cutoff filter to block the UV light (<400 nm) was used. As shown in figure 8 e, the photocatalytic reaction rate of $Fe_3O_4@TiO_2@Au$ (2120/MS) is 0.018 min^{-1}, which is 30 times larger than P25 (0.006 min^{-1}).

As shown in figure 8 f, pure TiO_2 (such as P25), is known to possess low photocatalytic activity under visible light irradiation (λ >400 nm).[45,46] The improvement of the catalytic performance is evident for $Fe_3O_4@TiO_2@Au$ (2120/MS), this is mainly attribute to the charge transfer from Ag to TiO_2 and the plasmon resonance energy transfer (PRET) from Ag to TiO_2.[32,47] On the one hand, the Au NPs can also been excited due to plasmon absorption under visible light, the resulting photogenerated electrons may transfer from the Au NPs to TiO_2's conduction band, resulting in the efficient electron-hole separation and possible oxidation reactions on the surfaces of as-prepared MS. On the other hand, the transfer of energy from a plasmon to the nearby TiO_2 (which has been called PRET) can enhance the electric field intensity in a small, well-defined location of the TiO_2, thereby results in the rapid formation of e$^-$/h$^+$ pairs in the TiO_2. Thus, the $Fe_3O_4@TiO_2@Au$ MS can achieve the self-cleaning property under both UV and visible light irradiation, this highlights one of advantages of the as-prepared multifunctional

MS, which is considered to be a convenient recyclable SERS substrate.

3.4. Regeneration activities of the triplex $Fe_3O_4@TiO_2@Au$ core-shell MS

As discussed above, one of the main advantages of as-prepared $Fe_3O_4@TiO_2@Au$ MS in comparison to other SERS substrates is their potential recyclability. If the obtained $Fe_3O_4@TiO_2@Au$ MS can clean fully itself by photocatalytic degradation of target molecules absorbing onto it, it can be re-used for further detection. After the substrate was detected, it was immersed in deionized water and irradiated with a Xenon lamp with a cutoff filter to block the UV light (<400 nm, 50 mW cm^{-2}) at room temperature to degrade the R6G molecules, and then the MS was washed with deionized water and collected by magnet. Finally, the MS were dried at 80 °C for further detection.[48] Figure 9 shows the results for R6G collected at the initial SERS detection and after self-cleaning treatment. As can be seen, the $Fe_3O_4@TiO_2@Au$ (2120/MS) shows great SERS activity, and after 90 min of visible light irradiation, the main bands of R6G lose intensity, which suggests that the R6G molecules can be removed. The as-prepared $Fe_3O_4@TiO_2@Au$ (2120/MS) are similar to that of a new substrate even after three recycles, indicating that the $Fe_3O_4@TiO_2@Au$ (2120/MS) are feasible to use as a recyclable SERS substrates.
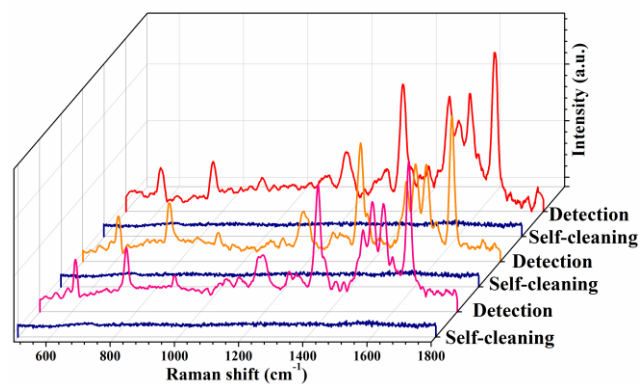
Figure 9. Raman spectra of three adsorption/UV cleaning cycles of R6G (10^{-5} M). Each cycle consists of adsorption of the target solution followed by visible light irradiation. The graph shows the Raman spectra before and after cleaning.
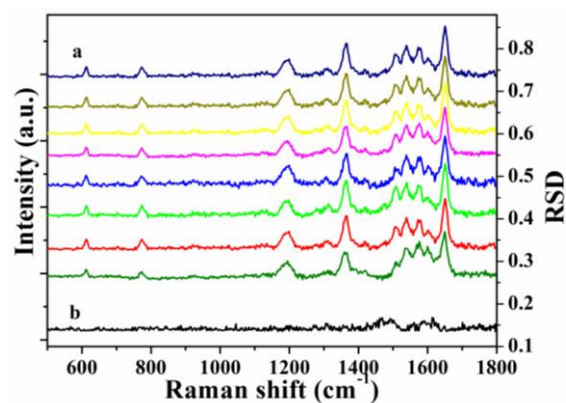
Figure 10. (a) a series of SERS spectrum of R6G molecules collected on randomly selected 9 places of $Fe_3O_4@TiO_2@Au$ (2120/MS) and (b) the corresponding RSD value curve.
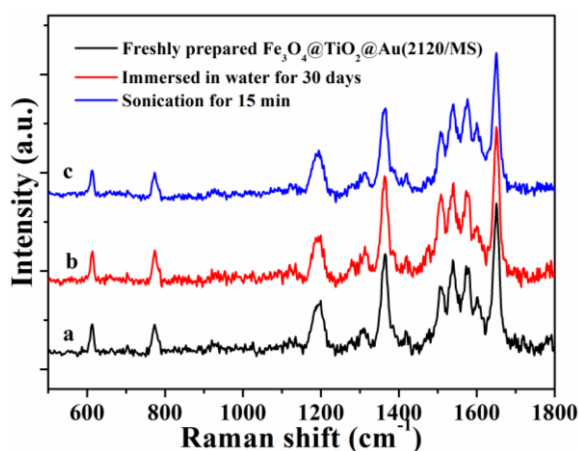
Figure 11. SERS spectra of R6G molecules obtained from (a) freshly prepared substrate and (b) the substrate immersed in water for 30 days and (c) the substrate sonication for 15 min.

As a recyclable SERS substrate, reproducibility and stability of SERS substrate must be validated.[49] First of all, the relative standard deviation (RSD) of major peaks is often used to estimate the reproducibility of SERS singnal.[50] Figure 10 shows the SERS-RSD spectura of R6G molecules, randomly collected from 9 positions of the substrate. The maximal RSD value of signal intensities of major SERS peaks was observed to be below 0.18, indicating that the as-prepared $Fe_3O_4@TiO_2@Au$ (2120/MS) has a good reproducibility across the entire area. Furthermore, in order to study the stability of the as-prepared $Fe_3O_4@TiO_2@Au$ (2120/MS) substrates, the MS were immersed in water for 30 days or sonication for 15 min and then performed SERS measurement on them. As shown in figure 11, neither a shift in the major Raman peaks nor a significant change in Raman intensity occurred for both of the two samples, indicating that the as-prepared MS shows great stability.

4. Conclusions

In conclusion, we have successfully synthesized the novel multifunctional $Fe_3O_4@TiO_2@Au$ triplex core-shell magnetic microspheres with different size and distribution of Au nanoparticles. The as-prepared microspheres show good SERS activity with high reproducibility and stability. Furthermore, due to possessing excellent catalytic and magnetic properties, the microspheres can clean themselves and can be re-used for several cycles with convenient magnetic separability. We have investigated the optimum size and distribution of Au nanoparticles to induce the maximum SERS activity, the $Fe_3O_4@TiO_2@Au$ (2120/MS) exhibits the enhancement ability of SERS for R6G with the detection limit of 10^{-11} M. The low signal interference of this effective method has shown a potential application for $Fe_3O_4@TiO_2@Au$ nanocomposites in different analytes, and the unique recyclable substrate provides a new way in eliminating the single-use problem of traditional SERS substrates. Additionally, these triplex core-shell magnetic microspheres can be extended to applications in other fields such as electromagnetic devices to biomedicine, catalysis, sensor, energy conversion, and so on.

Acknowledgements

References

Key Laboratory for Ultrafine Materials of Ministry of Education, School of Materials Science and Engineering, East China University of Science and Technology, Shanghai 200237, China. Fax: +86 21 6425 0624; Tel: +86 21 6425 2022; E-mail: yhzhu@ecust.edu.cn (Y. Zhu); czli@ecust.edu.cn (C. Li).

1   W. E. Smith, *Chem. Soc. Rev.*, 2008, **37**, 955.
2   S. M. Nie and S. R. Emory, *Science*, 1997, **275**, 1102.
3   M. D. Porter, R. J. Lipert, L. M. Siperko, G. Wang, R. Narayanan, *Chem. Soc. Rev.*, 2008, **37**, 1001.
4   J. N. Anker, W. P. Hall, O. Lyandres, N. C. Shah, J. Zhao and R. P. Van Duyne, *Nature Mater.*, 2008, **7**, 442.
5   Y. W. C. Cao, R. C. Jin and C. A. Mirkin, *Science*, 2002, **279**, 1536.
6   J. R. Lombardi and R. L. Birke, *Acc. Chem. Res.*, 2009, **42**, 734.
7   M. C. Shen, C. Hui, T. Z. Yang, W. C. Xiao, J. F. Tian, L. H. Bao, S. T. Chen, H. Ding and H. Gao, *J. Chem. Mater.*, 2008, **20**, 6939.
8   L. Yoon, T. Kang, W. Choi, J. Kim, Y. Yoo, S.. W. Joo, Q. H. Park, H. Ihee and B. Kim, *J. Am. Chem. Soc.*, 2009, **131**, 758.
9   H. J. Chen, Y. L. Wang and S. J. Dong, *J. Raman Spectrosc.*, 2009, **40**, 1188.
10 H. M. Song, L. Deng and N. M. Khashab, *Nanoscale*, 2013, **5**, 4321.
11 N. L. Netzer, C. Qiu, Y. Y. Zhang, C. K. Lin, L. F. Zhang, H, Fong and C. Y. Jiang, *Chem. Commun.,* 2011, **47**, 9606-9608.
12 H. Y. Liang, Z. P. Li, W. Z. Wang, Y. S. Wu and H. X. Xu, *Adv. Mater.*, 2009, **21**, 4614.
13 J. Xie, Y. Lee, D. I. C. Wang and Y. P. Ting, *Small*, 2007, **3**, 672.
14 X. T. Bai and L. Q. Zheng, *Cryst. Growth Des.*, 2010, **10**, 4701.
15 Y. Q. Wang, K. Wang, B. F. Zou, T. Gao, X. L. Zhang, Z. L. Du and S. M. Zhou, *J. Mater. Chem. C.*, 2013, **1**, 2441.
16 L. B. Yang, X. Jiang, W. D. Ruan, J. X. Yang, B. Zhang, W. Q. Xu and J. R. Lombardi, *J. Phys. Chem. C.*, 2009, **113**, 16226.
17 G. Sinha, L. E. Depero and I. Alessandri, *Acs Appl. Mater. Interface*, 2011, **3**, 2557.
18 W. C. Cheng, B. Yan, S. M. Wong, X. L. Li, W. W. Zhou, T. Yu, Z. X. Shen, H. Y. Yu and H. J. Fan, *J. ACS Appl. Mater. Interface*, 2010, **2**, 1824.
19 I. Alessandri and L. E. Depero, *Chem. Commun.,* 2009, **17**, 2359.
20 L. B. Yang, X. Jiang, W. D. Ruan, B. Zhao, W. Q. Xu and J. R. Lombardi, *J. Phys. Chem .C.*, 2008, **112**, 20095.
21 W. Ji, X. X. Xue, W. D. Ruan, C. X. Wang, N. Ji, L. Chen, Z. S. Li, W. Somg, B. Zhao and J. R. Lombardi. *Chem. Commun.*, 2011, **47**, 2426.
22 S. G. Rebecca, E. D. William and J. N. Michael, *ACS Nano*, 2009, **3**, 2859.
23 C. X. Wang, W. D. Ruan, N. Ji, W. Ji, S. Lv, C. Zhao and B. Zhao, *J. Phys. Chem. C.*, 2010, **114**, 2886.
24 Y. Zhou, J. Chen, L. Zhang and L. B. Yang, *Eru. J. Inorg. Chem.*, 2012, **19**, 3176.
25 J. F. Li, Y. Cui, M. Gao, J. Luo, Y. Ding, Z. L. Yang, S. B. Li, X. S. Zhou, F. R. Fan, W. Zhang, Z. Y. Zhou, D. Y. Wu, B. Ren, Z. L. Wang and Z. Q. Tian, *Nature*, 2010, **464**, 392.
26 A. K. Charkraborty, Z. Qi, S. Y. Chai, C. Lee, S. Park, D. Jiang and W. L. Lee, *Appl. Catal. B Env.*, 2010, **93**, 368.
27 X. X. Zou, .R Silva, X. X. Huang, J. F. Al-Sharab and T. Asefa, *Chem. Commun.*, 2013, **49**, 382.
28 J. H. Shen, Y. H. Zhu, X. L. Yang, J. Zong and C.Z. Li. *Langmuir*, 2013, **29**, 690.
29 Y. Q. Wang, B. F. Zou, T. Gao, X. P. Wu, X. P. Wu, S. Y. Lou and S. M. Zhou, *J. Mater. Chem.*, 2012, **22**, 9034.
30 H. Jun, M. S. Noh, G. Kim, H. Kang, W. J. Chuang, Y. K. Kim, M. H. Cho, D. H. Jeong and Y. S. Lee, *Anal. Biochem.*, 2009, **391**, 24.
31 R. Liu, Y. L. Guo, G. Qdusote, F. L. Qu and R. D. Priestley. *ACS Appl. Mater. Interface*, 2013, **5**, 9167.

32   X. Q. Zhang, Y. H. Zhu, X. L. Yang, S. W. Wang, J. H. Shen, B. B. Lin and C. Z. Li, *Nanoscale*, 2013, **5**, 3359.

33   J. Liu, Z. K. Sun, Y. H. Deng, Y. Zou, C. Y. Li, X. H. Guo, L. Q. Xiong, Y. Gao, Y. F. Li and D. Y. Zhao, *Angew. Chem. Int. Ed.*, 2009, **48**, 5875.

34   W. Li, J. P. Yang, Z. X. Wu, J. X. Wang, B. Li, S. S. Feng, Y. H. Deng, F. Zhang and D. Y. Zhao, *J. Am. Chem. Soc.*, 2012, **134**, 11864.

35   J. Kimling, M. Maier, B. Okenve, V. Kotaidis, H. Ballot and P. Plech, *J. Phys. Chem. B*, 2006, **110**, 15700.

36   C. Ziegler and A. Eychmuller, *J. Phys. Chem. B*, 2011, **115**, 4502.

37   S. T. Kochuveedu, D. P. Kim and D. H. Kim, *J. Phys. Chem. C*, 2012, **116**, 2500.

38   Y. X. Hu and Y. G. Sun, *J. AM. Chem. Soc.*, 2013, **135**, 2213.

39   C. W. Cheng, B. Yan, S. M. Wong, X. L. Li, W. W. Zhou, T. Yu, Z. X. Shen, H. Y. Yu and H. J. Fan, *ACS Appl, Mater. Interfaces*, 2010, **2**, 1824.

40   J. Xie, Q. Zhang, J. Y. Lee and D. I. C. Wang, *ACS Nano*, 2008, **2**, 2473.

41   S. J. Zhuo, M. W. Shao and S. T. Lee, *ACS Nano*, 2012, **6**, 1059.

42   X. D. Wang, T. Dornon, M. Blackford and R. A. Caruso, *J. Mater. Chem.*, 2012, **22**, 11701.

43   O. Akhavan and E. Ghaderi, *Surf. Coat. Technol.*, 2010, **204**, 3676.

44   X. D. Wang and R. A. Caruso, *J. Mater, Chem.*, 2011, **21**, 20.

45   O. Akhavan and R. Azimirad, *Appl. Catal., A*, 2009, **369**, 77.

46   O. Akhavan, R. Azimirad, S. Safa and M. M. Larijani, *J. Mater. Chem.*, 2010, **20**, 7386.

47   S. C. Warren and E. Thimsen, *Energy Environ. Sci.*, 2012, **5**, 5133.

48   X. L. Yang, H. Zhong, Y. H. Zhu, J. H. Shen and C. Z. Li, Dalton Trans., 2013, **42**, 14324.

49   X. H. Li, G. Y. Chen, L. B. Yang, Z. Jin and J. H. Liu, *Adv. Funct. Mater.,* 2010, **20**, 2815.

50   B. H. Zhang, H. S. Wang, L. H. Lu, K. L. Ai, G. Zhang and X. L. Cheng, *Adv. Funct. Mater.*, 2008, **18**, 2348.